Charge radii of thallium isotopes near the $N = 126$ shell closure

Z. Yue,[1,*] A. E. Barzakh,[†] A. N. Andreyev,[1,2,‡] I. N. Borzov,[§] J. G. Cubiss,[1] A. Algora,[3] M. Au,[2,4] M. Balogh,[5] S. Bara,[6] R. A. Bark,[7] C. Bernerd,[2,6] M. J. G. Borge,[8] D. Brugnara,[5] K. Chrysalidis,[2,4] T. E. Cocolios,[6] H. De Witte,[6] Z. Favier,[2] L. M. Fraile,[9] H. O. U. Fynbo,[10] A. Gottardo,[5] R. Grzywacz,[11] R. Heinke,[2] A. Illana,[9,12,13] P. M. Jones,[7] D. S. Judson,[14] A. Korgul,[15] U. Köster,[2,16] M. Labiche,[17] L. Le,[2] R. Lica,[2,18] M. Madurga,[11] N. Marginean,[18] B. A. Marsh,[2] C. Mihai,[18] E. Nácher,[3] C. Neacsu,[18] C. Nita,[18] B. Olaizola,[2,8] J. N. Orce,[19] C. A. A. Page,[1] R. D. Page,[14] J. Pakarinen,[2,12,13] P. Papadakis,[17] A. Perea,[8] M. Piersa-Siłkowska,[20] Zs. Podolyák,[2,21] E. Reis,[2,22] S. Rothe,[2] M. Sedlak,[5] C. Sotty,[18] S. Stegemann,[2] O. Tengblad,[8] S. V. Tolokonnikov,[§] J. M. Udías,[9] P. Van Duppen,[6] N. Warr,[23] and W. Wojtaczka[6]
(IDS Collaboration)

[1]*School of Physics, Engineering and Technology, University of York, York YO10 5DD, United Kingdom*
[2]*CERN, 1211 Geneva 23, Switzerland*
[3]*Instituto de Fisica Corpuscular, CSIC-Universidad de Valencia, E-46071 Valencia, Spain*
[4]*Johannes Gutenberg-Universität, Saarstr. 21, 55099 Mainz, Germany*
[5]*INFN, Laboratori Nazionali di Legnaro (LNL), Viale dell'Università 2, 35020 Legnaro (PD), Italy*
[6]*Instituut voor Kern- en Stralingsfysica, KU Leuven, B-3001 Leuven, Belgium*
[7]*iThemba LABS, National Research Foundation, P.O. Box 722, Somerset West 7129, South Africa*
[8]*Instituto de Estructura de la Materia, CSIC, 28006 Madrid, Spain*
[9]*Grupo de Física Nuclear and IPARCOS, Universidad Complutense de Madrid, CEI Moncloa, E-28040 Madrid, Spain*
[10]*Department of Physics and Astronomy, Aarhus University, DK-8000 Aarhus C, Denmark*
[11]*Department of Physics and Astronomy, University of Tennessee, Knoxville, Tennessee 37966, USA*
[12]*Department of Physics, University of Jyväskylä, P.O. Box 35, FI-40014 Jyväskylä, Finland*
[13]*Helsinki Institute of Physics, University of Helsinki, P.O. Box 64, FIN-00014 Helsinki, Finland*
[14]*Oliver Lodge Laboratory, University of Liverpool, Liverpool L69 7ZE, United Kingdom*
[15]*Institute of Experimental Physics, Warsaw University, Warszawa PL 00-681, Poland*
[16]*Institut Laue-Langevin, F-38042 Grenoble, France*
[17]*STFC Daresbury Laboratory, Daresbury, WA4 4AD Warrington, United Kingdom*
[18]*Horia Hulubei National Institute of Physics and Nuclear Engineering (IFIN-HH), R-077125 Bucharest, Romania*
[19]*Department of Physics, University of the Western Cape, P/B X17 Bellville 7535, South Africa*
[20]*Institute of Experimental Physics, Warsaw University, Warsaw PL 02-093, Poland*
[21]*Department of Physics, University of Surrey, Guildford GU2 7XH, United Kingdom*
[22]*Universität Duisburg-Essen, 45141 Duisburg, Germany*
[23]*Institut für Kernphysik, Universität zu Köln, D-50937 Köln, Germany*

(Received 20 July 2024; accepted 27 August 2024; published 13 September 2024)

The changes in the mean-squared charge radius of ^{209}Tl^{g} ($N = 128$) and ^{207}Tl^{m} ($N = 126$) relative to ^{205}Tl have been measured for the first time using the in-source laser resonance-ionization spectroscopy technique with the Laser Ion Source and Trap (LIST) at ISOLDE (CERN). The application of the LIST suppresses the dominant background from isobaric francium isotopes and allows access to thallium nuclides with $A \geqslant 207$. The characteristic kink in the charge radii at the $N = 126$ neutron shell closure, as well as the odd-even effect similar to that in the adjacent bismuth, lead, and mercury isotopic chains, have been observed. The self-consistent theory of finite Fermi systems based on the energy density functional by Fayans *et al.* reproduces the behavior of charge radii in these isotopic chains near $N = 126$. The comparison with calculations in the framework of the relativistic mean field (RMF) approach is also presented. In the case of the Fayans functional it is a specific form of pairing interaction with the dependence on the density gradient that is essential to provide agreement with the

*Contact author: zixuan.yue@cern.ch
†Contact author: barzakh_ae@pnpi.nrcki.ru; Affiliated with an institute covered by a cooperation agreement with CERN at the time of the experiment.
‡Contact author: andrei.andreyev@york.ac.uk
§Affiliated with an institute covered by a cooperation agreement with CERN at the time of the experiment.

experimental charge radii. In particular, the kink is reproduced without the inversion of $g_{9/2}$ and $i_{11/2}$ neutron single-particle states, which is a prerequisite to correctly describe the kink in the RMF models.

DOI: 10.1103/PhysRevC.110.034315

I. INTRODUCTION

It is well established that the slope of the change in the mean-squared charge radii ($\delta\langle r^2\rangle$) along isotopic chains increases abruptly when crossing the neutron magic numbers (the so-called "kink in charge radii" or "shell effect in radii" [1,2]). This effect proved to have an universal character being observed near almost all neutron magic numbers including $N = 126$ [1,2].

Another universal trend in the charge-radii behavior is the odd-even staggering (OES): in most cases, nuclear charge radii of odd-N isotopes are smaller than the average of their even-N neighbors [1,2]. A few exceptions are usually explained by the influence of the static (quadrupole or octupole) deformation (see Refs. [3,4] and references therein).

In the vicinity of the $N = 126$ and $Z = 82$ shell closures, well-documented evidence for the kink exists for the mercury ($Z = 80$) [5,6], lead ($Z = 82$) [7], and bismuth ($Z = 83$) [8] isotopic chains. This region is especially suitable to compare of different theoretical approaches for describing the kink and OES, since the deformation effects which could distort these $\delta\langle r^2\rangle$ trends, are expected to be small. This is in contrast with, e.g., the situation near $N = 82$ where rapid growth of deformation in the close vicinity of the magic number was observed (see, for example, Fig. 4 in Ref. [9] and experimental data compilation in Ref. [10]).

Correspondingly, the first aim of the present work is to fill the $Z = 81$ gap in the $\delta\langle r^2\rangle$ systematics near $N = 126$ by measuring $\delta\langle r^2\rangle$ for thallium isotopes ($Z = 81$) with $N > 127$. These values are derived from the isotope shifts (IS) of the atomic optical lines.

Previously, IS and hyperfine structure (hfs) in neutron-deficient thallium isotopes down to ^{179}Tl were studied [11–13] using the resonance ionization laser ion source technique [14]. Isotopes with $N > 127$ remained inaccessible due to the overwhelming surface-ionized isobaric francium contamination. The application of the resonance-ionization spectroscopy in the Laser Ion Source and Trap (LIST) [15–17] in the present work suppresses this background and provides access to heavy thallium isotopes.

The determination of the $\delta\langle r^2\rangle$ values for thallium isotopes with $N > 126$ also probes the possible role that low-j proton orbitals could play in producing the kink. Indeed, for the bismuth isotopic chain above $Z = 82$, it is the high-j $h_{9/2}$ proton orbital that dominates the structure of the ground state, while the low-j $s_{1/2}$ orbital is active in ground states of thallium isotopes.

Historically, considerable theoretical efforts have been directed to the description of the kink in the lead chain around $N = 126$. It was found that standard nonrelativistic Hartree-Fock (NRHF) calculations with Skyrme or Gogny forces were not able to reproduce the kink [18–20]. Further numerous attempts to take into account ground-state correlations using beyond mean-field approaches (random phase approximation, generator-coordinate method, self-consistent sum rule approach) fail to reproduce the observed irregularity (see Refs. [9,19,21,22] and references therein).

The OES also became a benchmark to test the theoretical models. As in the case of the kink, the first theoretical attempts tried to account for a reduction of quadrupole vibrations in odd-N nuclei due to blocking, which can be regarded as a kind of beyond mean-field approach. However, experimental data were only qualitatively explained within the corresponding pairing-plus-quadrupole model for spherical nuclei [23].

The failure of the beyond Hartree-Fock attempts to explain the kink and OES, indicates that a correct description of IS (at least in the NRHF calculations) is not determined by the higher-order correlations and a solution should be searched for through the modification of the effective forces themselves [19]. In particular, it was shown that the experimental kink and OES can be reproduced in the framework of the Skyrme-Hartree-Fock (SHF) approach with a density-dependent parametrization of the pairing part of the interaction [19,24] or with the modification of the spin-orbit interaction, see Refs. [20,25–29]. However, it was shown that it remains difficult to reproduce both the masses and the kink accurately within one SHF framework with the generalization of the spin-orbit interaction [30]. In the case of the pairing modification it also remains unclear whether the modified functionals provide an accurate global description of nuclear masses.

At the same time, both kink and OES are well reproduced in the framework of the relativistic mean field (RMF) approach without introducing new functional members or adjusting parameters ([18,31], see also comprehensive reviews which covers nearly the whole nuclide chart [32,33]). However, this success is achieved at the expense of the inversion of the $\nu i_{11/2}$ and $\nu g_{9/2}$ neutron single-particle states position in contradiction with experiment [5,6,32].

In contrast with the theoretical approaches discussed above, in the self-consistent finite Fermi systems theory (TFFS) [34] based on the generalized energy density functional (EDF) by Fayans *et al.* [21,35–38], nuclear radii in the vicinity of the neutron shell closures are directly included in the optimization protocol. Two recent versions of the Fayans-type functional (DF3-a [37] and Fy(Δr, HFB) [38]) successfully describe the shell effect in radii and OES for K [39,40], Ca [38,41], Cu [42,43], Sn [44], Ca-Zn [45], and some other isotopic chains. In contrast with the RMF calculation, in the TFFS-Fayans framework the kink is reproduced without the inversion of the $\nu i_{11/2}$ and $\nu g_{9/2}$ states. Thus, we have two main competitive approaches for describing the kink and OES: RMF and nonrelativistic Fayans-functional theories [46]. It is important that both approaches describe these peculiarities of the $\delta\langle r^2\rangle$ behavior without loss of accuracy in the reproduction of the nuclear masses in contrast with the majority of the (modified) NRHF approaches [38,47]. In the case of the Fayans functional it is a specific form of pairing

interaction with the dependence on the density gradient that is essential to provide agreement with the experimental charge radii [35,44], whereas the kink and OES are already present in the RMF calculations without pairing [5,6].

This contradiction encourages a more detailed comparison between these theories for the kink and OES. Such an analysis is the second aim of the present work whereby we used the advanced RMF approaches summarized in Ref. [33] with the PC-L3R [48], PC-X [49], DD-MEX [49], and DD-PCX [50] interactions. The calculations with (modified) DF3-a Fayans-type functional were made specifically for the present work.

II. EXPERIMENTAL DETAILS

The data presented in this work originate from the same experiment as described in Ref. [51], and therefore only the most relevant details will be given here.

Radioactive thallium isotopes were produced in spallation reactions by a 1.4-GeV proton beam (intensity up to 2 μA) from the CERN proton synchrotron booster bombarding a 50 g/cm^2 UC_x target. The reaction products diffused through the target material ($T \approx 2000$–$2200\,^\circ$C), and effused into the hot cavity of the target-ion source device as neutral atoms. At the masses of interest ($A = 207$–209), strong isobaric contamination from surface-ionized francium is present, which prevented extensions of earlier experiments with thallium [11–13] to heavier masses.

To overcome this problem, the LIST device was used [15–17]. In our experiment, the francium ions were suppressed by a factor of $\approx 10^4$. At the same time, the laser-ionized thallium isotopes were suppressed by a factor of ≈ 20, relative to normal laser ion source operation without the LIST [14]. The improved signal-to-background ratio due to the suppression of the surface-ionized francium (see details in Ref. [51]) was the key condition which allowed us to perform our measurements.

Inside the LIST, thallium atoms were resonantly ionized using the two-step thallium ionization scheme [11–13,51]. For IS measurement the first step 277-nm $6p\ ^2P_{1/2} \rightarrow 6d\ ^2D_{3/2}$ atomic transition was scanned by a frequency-doubled tunable dye laser (LIOP-TEC LiopStar) beam with a linewidth of ≈3 GHz. The subsequent ionization step was provided by a frequency doubled Nd : YVO_4 laser (Lumera Blaze, fundamental frequency of 532 nm).

After ionization, the thallium ions were extracted and accelerated by a 50-kV electrostatic potential, and mass-separated by the ISOLDE general purpose separator. The ions were then delivered to either a Faraday cup (FC) or the ISOLDE Decay Station (IDS) [52] for ion counting. The ion current of the stable isotopes ^{203,205}Tl from a dedicated oven, as well as abundantly produced ^{207}Tl^g, were directly measured by the FC. ^{205}Tl was used as the reference isotope for the IS measurements.

III. DATA ANALYSIS AND RESULTS

A. Fitting of the hyperfine-structure spectra

Examples of the hfs spectra are shown in Fig. 1. This figure is modified from Fig. 1 of Ref. [51] by adding the

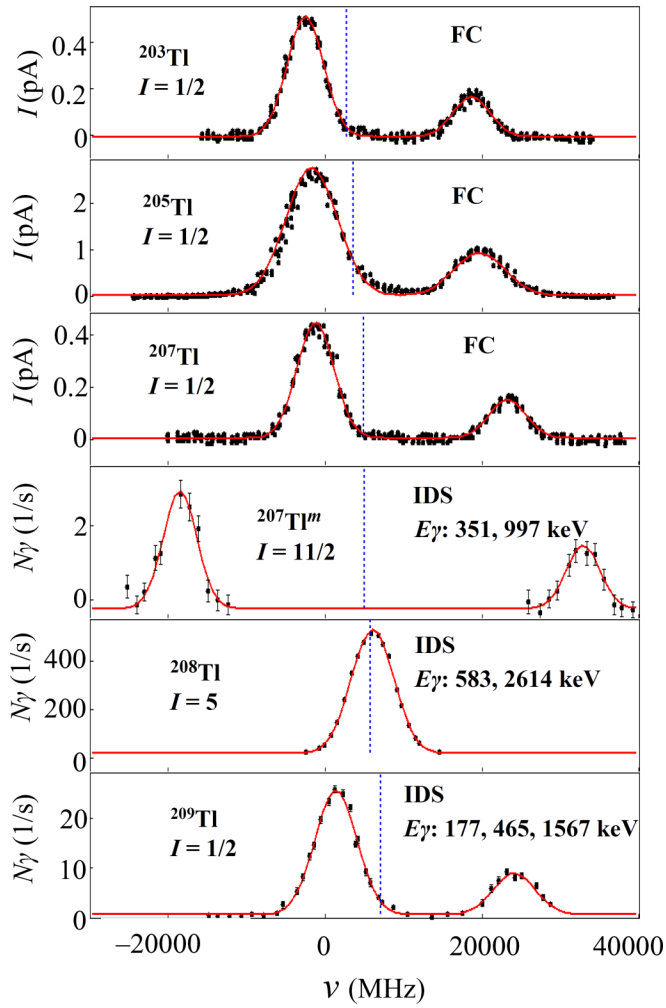

FIG. 1. Examples of the hfs spectra of studied thallium isotopes. The solid red lines are Voigt profile fits of the data. Vertical dotted lines mark centers of gravity of the corresponding hfs. The nuclear spin and photoion detection method (FC or IDS), as well as γ-ray energies in the case of decay-based detection at IDS, are displayed for each isotope. The zero point on the frequency scale corresponds to a wave number of 36117.92 cm^{-1}.

^{208}Tl hfs. The data analysis procedure was the same as in our previous studies of the neutron-deficient thallium isotopes [12,13]. The positions of the hyperfine components in the hfs spectra are determined by the standard relation [12] with five parameters: nuclear spin (I), isotope shift relative to the stable ^{205}Tl ($\delta\nu^{A,205}_{277\text{nm}}$), magnetic hfs constants (a_1 and a_2) for the first and the second level of the ionization scheme, and the electric quadrupole hfs constant b_2 for the second level. Note that $b_1 \equiv 0$, since the first level in our ionization scheme has electronic angular momentum $J = 1/2$.

Voigt profiles were fitted to the experimental hfs spectra using a fixed $a_2/a_1 = -0.002013(19)$ ratio taken from the value for the stable isotopes ^{205}Tl [53], and I values from [54]. For ^{208}Tl, the constant a_1 taken from Ref. [55], was fixed.

For ^{207}Tl^m with $I = 11/2$, the possible quadrupole splitting of the upper level $6d\ ^2D_{3/2}$ of the scanned transition was

TABLE I. Isotope shifts for the 277-nm transition ($\delta\nu^{A,205}$) and changes in mean-squared charge radius ($\delta\langle r^2\rangle^{A,205}$) of thallium isotopes with $A > 200$. The statistical experimental uncertainties are given in parentheses. The values in curly brackets are the systematic errors which stem from the uncertainty of the F and k_{MS} factors. Where available, literature values are shown in italic in a second line for each isotope.

A	I^π	$\delta\nu^{A,205}$(MHz)	$\delta\langle r^2\rangle^{A,205}$(fm^2)
203	$1/2^+$	−1026(104)	−0.107(11){3}
		−1038.5(1) [53]	*−0.10840(3){220}* [56]
207	$1/2^+$	1023(175)	0.107(19){3}
		1030(240) [12]	*0.1100(2){22}* [56]
207m	$11/2^-$	1030(290)	0.108(31){3}
208	5^+	2118(190)	0.223(21){6}
			0.192(13){4} [56]
			0.201(14)[a]
209	$1/2^+$	3130(220)	0.330(23){8}

[a]Weighted mean for $\delta\langle r^2\rangle^{208,205}$ between our result and that from Ref. [56].

taken into account using advanced atomic calculations of the electric field gradient produced by the electrons at the site of the nucleus [51].

B. Changes in mean-squared charge radii

The $\delta\langle r^2\rangle$ values were deduced using the standard parametrization of the isotope shift $\delta\nu^{A',A} = \nu^{A'} - \nu^{A}$ [57]:

$$\delta\nu^{A',A} = k_{\mathrm{MS}}\left(\frac{1}{M^{A'}} - \frac{1}{M^{A}}\right) + F\delta\langle r^2\rangle^{A',A}. \quad (1)$$

Here, k_{MS} and F are the mass- and field-shift constants, respectively, M^A and $M^{A'}$ are the atomic masses of isotopes with mass number A and A', and $\delta\langle r^2\rangle^{A',A} = \langle r^2\rangle^{A'} - \langle r^2\rangle^{A}$ is the difference between their nuclear mean-squared charge radii.

In this work, we have used $F = 9.32(23)\,\mathrm{GHz/fm^2}$, $k_{\mathrm{MS}} = -575(71)\,\mathrm{GHz\,u}$, which were recently calculated in Ref. [56] accounting for relativistic and high-order electronic correlation effects.

In Table I, the IS for the 277-nm transition and $\delta\langle r^2\rangle$ for the studied thallium isotopes are shown, along with values from literature. Our results for ^{203,207}Tl^g agree with the literature data. For ^{208}Tl our value differs from the literature by 1.2σ and the weighted mean of the literature data and that from our measurements is used below. Figure 2 shows the $\delta\langle r^2\rangle$ values for thallium nuclei near $N = 126$. As seen in Table I, the radii for ^{207}Tl^g ($I = 1/2$) and ^{207}Tl^m ($I = 11/2$) are the same within uncertainties, and would be indistinguishable in Fig. 2, therefore only the $\delta\langle r^2\rangle$ for ^{207}Tl^g is shown.

The behavior of charge radii in Hg, Tl, Pb, and Bi isotopic chains near $N = 126$ is strikingly similar as seen in Fig. 3. (See also the discussion on the kink indicator in Sec. V.) In contrast to the kink at $N = 82$ (see Fig. 4 in Ref. [9], for example), the kink at $N = 126$ has no clear Z dependence, at least within the limits of the current experimental uncertainties. Thus, there is no notable difference between

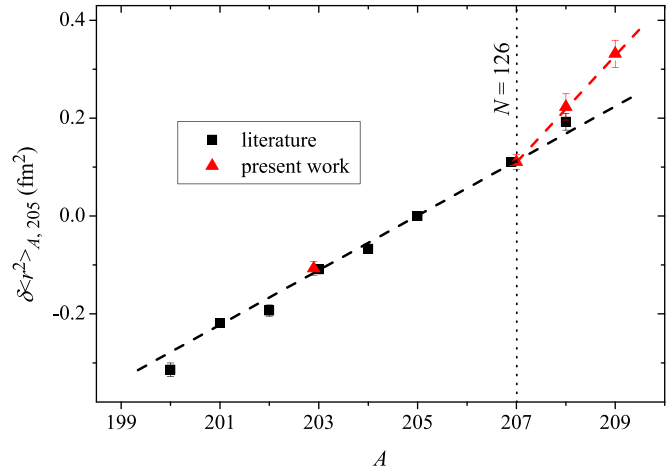

FIG. 2. The $\delta\langle r^2\rangle$ values for thallium isotopes near $N = 126$. The red triangles are results from the present work, and the black squares are literature values taken from [56]. The values for even-N nuclei are connected by the dashed line to guide the eyes. The uncertainties include both statistical and systematic ones.

the cases where valence protons occupy low-j orbitals, such as in thallium ($s_{1/2}$), and high-j ones as in bismuth ($h_{9/2}$). The independence of the kink on the orbital occupied by the valence proton is supported by the negligible isomer shift for ^{207}Tl^m ($I = 11/2, \pi h_{11/2}$) relative to ^{207}Tl^g ($I = 1/2, \pi s_{1/2}$) (see Table I).

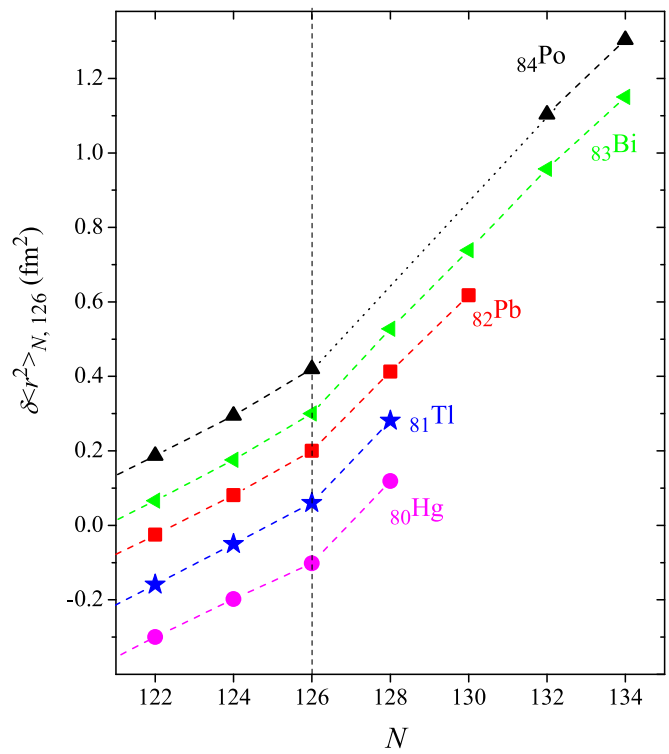

FIG. 3. The $\delta\langle r^2\rangle$ values for the isotopic chains with Z close to $Z = 82$ in the vicinity of $N = 126$. Only even-N isotopes are shown for more distinct kink presentation.

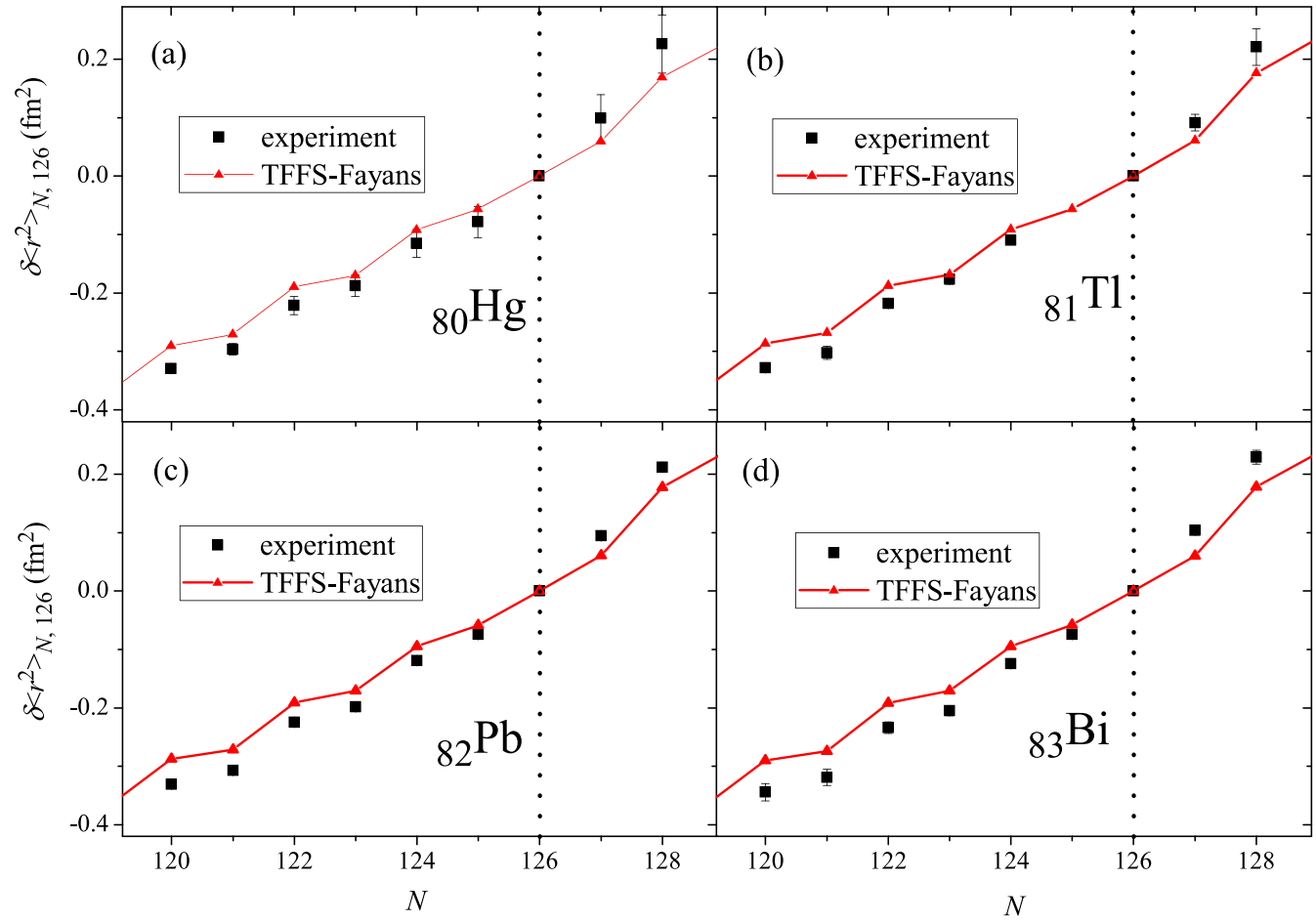

FIG. 4. Comparison of the TFFS-Fayans calculations for $\delta\langle r^2\rangle$ values with the experiment for the $_{80}$Hg, $_{81}$Tl, $_{82}$Pb, and $_{83}$Bi isotopic chains near $N = 126$. Experimental data are taken from (a) Refs. [3,5,6]; (b) Ref. [56] and present work; (c) Ref. [7]; (d) Refs. [8,58].

IV. THEORETICAL CALCULATIONS

The experimental data were compared with calculations in the framework of the finite Fermi system theory, based on the generalized EDF method implemented with the DF3-a functional by Fayans *et al.* [21,36,59]. Compared to the Skyrme or Gogny EDF it has a more complex (a fractional-linear) dependence on the particle densities.

The anomalous part of the Fayans functionals (see definitions in [21]) involves the attractive term accounting for pairing in the nuclear exterior and two repulsive surface terms depending on the particle densities and their gradients. The density-gradient dependent term is crucial for explaining the kink and OES effects in charge radii [21,35,36,44]. It is this term that made it possible to ensure in [21] that the ^{40}Ca and ^{48}Ca radii are approximately equal already at the mean-field level. A comparison with the results obtained in [60] confirms the fact that this gradient term effectively takes into account the phonon coupling effect on the charge-density distribution.

The effective density-dependent contact pairing with a cutoff at $E_{\rm Fermi}$ used in our calculations, is non-universal, therefore, a number of (A, Z-dependent) pairing parametrizations exists reflecting a complexity of interplay between the aforementioned terms. For the present kink and OES calculations, the functional parameters in the pairing sector were readjusted using the available neutron separation energies (S_n) and charge radii in mercury, thallium, lead, and bismuth isotopes. For a better simultaneous description of the S_n and kink data, the following parameter set was found: $f^{\xi} = -1.05$, $h^{\xi} = 0.78$, $f^{\xi}_{\nabla} = 1.25$ (designation of parameters was taken from [21]). This adjustment maintains a good description of binding energies and charge radii of spherical nuclei in the calcium, nickel and lead regions, to which the parameters of the DF3 and DF3-a functionals were fitted. In general, the global performance of the functional is comparable with the DF3-a pairing functional set [21,36].

V. DISCUSSION

As seen in Fig. 4, the TFFS calculations with the modified DF3-a functional satisfactorily describe the $\delta\langle r^2\rangle$ behavior in thallium isotopes (mean deviation is 0.03 fm^2). The theoretical results for adjacent $_{80}$Hg, $_{82}$Pb, and $_{83}$Bi chains demonstrate the similar agreement with experiment (see Fig. 4). It is important that the change of the pairing parameters does not worsen the description of the neutron separation energy as shown, e.g., for Pb and Tl chains in Fig. 5.

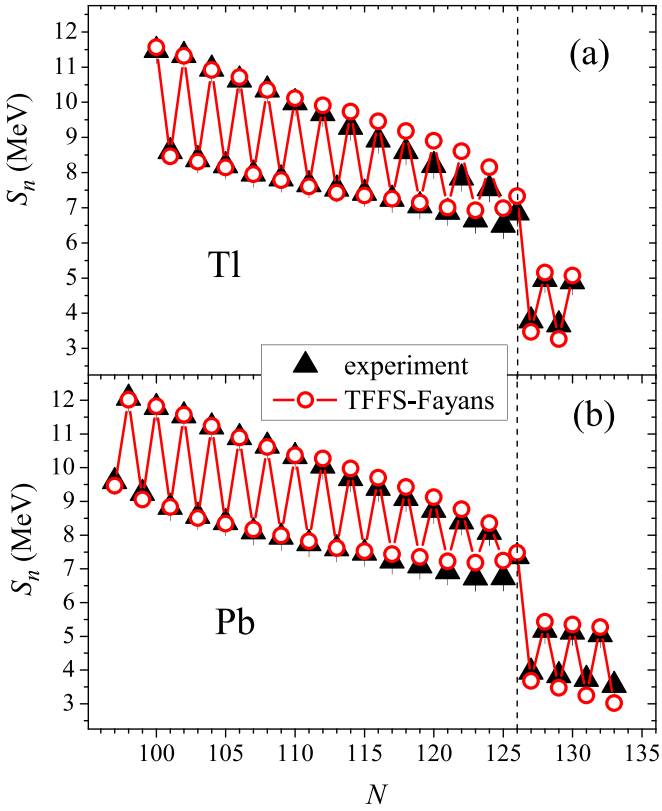

FIG. 5. Comparison of the TFFS-Fayans calculations of the neutron separation energy S_n with the experimental data for the $_{81}$Tl and $_{82}$Pb isotopic chains. Experimental data were taken from Ref. [61].

In order to quantitatively compare the magnitude of the kink and OES in different theoretical approaches, the kink (ξ) and staggering (γ_N) indicators were introduced:

$$\xi = \frac{\delta\langle r^2\rangle^{128,126}}{\delta\langle r^2\rangle^{126,124}}, \tag{2}$$

$$\gamma_N = \frac{2\delta\langle r^2\rangle^{N-1,N}}{\delta\langle r^2\rangle^{N-1,N+1}}. \tag{3}$$

Superscript indices point to the neutron numbers. These indicators are independent of the uncertainties in the atomic F factor (usually 5–10% in the lead region). The choice of the even-N isotope nearest to the neutron magic numbers for the kink indicator, helps to avoid mixing of the shell effect with other effects which might contribute to the observed $\delta\langle r^2\rangle$ value.

In Fig. 6 the experimental kink indicators for mercury, thallium, lead and bismuth isotopic chains are compared with theoretical results obtained within the RMF (PC-L3R, PC-X, DD-MEX, and DD-PCX functionals; see Ref. [33]) and Fayans-type (with improved DF3-a functional) approaches. The TFFS (DF3-a) calculations with modified pairing, excellently reproduce the experimental data, whereas the PC-L3R, PC-X, and DD-PCX functionals markedly overestimate the shell effect in radii and the DD-MEX functional predicts a noticeable Z dependence of the kink indicator which is not observed experimentally. However, one should keep in mind

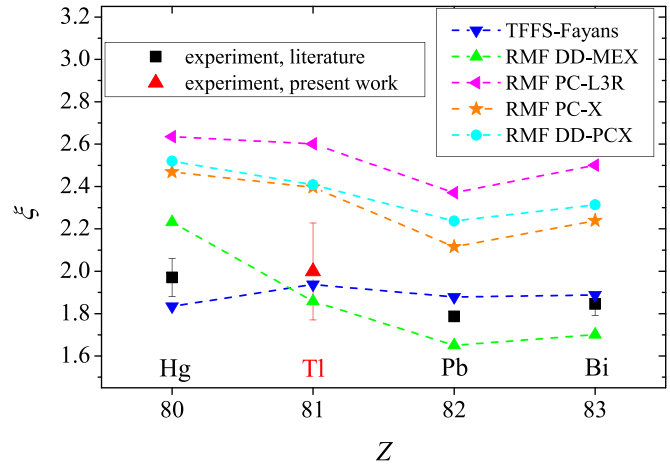

FIG. 6. Kink indicator for the isotopic chains near $Z = 82$. Experimental data are taken from Refs. [7] (Pb isotopes); [3,5,6] (Hg isotopes); [8,58] (Bi isotopes); [56] and present work (Tl isotopes). Theoretical values (RMF with different functionals) are derived from the calculation in Ref. [33].

that accounting for the center-of-mass corrections give sizable impacts on the charge radius and can improve description of kink in the RMF model [62].

It should be noted that the single-particle spectrum of neutrons in ^{208}Pb extracted from the excitation spectra of the neighboring odd isotopes ^{207}Pb and ^{209}Pb, is well reproduced in the TFFS-Fayans calculations (see Fig. 1 in Ref. [37]), whereas the RMF approach fails to reproduce the order of the neutron single-particle states near $N = 126$. In particular, in the RMF calculations the $\nu i_{11/2}$ state is lower in energy than the $\nu g_{9/2}$ state in contradiction with experiment [5,6,32]. In contrast with the RMF calculation, in the TFFS-Fayans approach the kink is reproduced without the inversion of the $\nu i_{11/2}$ and $\nu g_{9/2}$ states.

The contradiction of the RMF approach with experiment (inverted position of $\nu g_{9/2}$ and $\nu i_{11/2}$) is eliminated for odd-N nuclei by taking into account the coupling of single-particle motion with phonons (particle-vibration coupling) (see [63,64]). At the same time, in the RMF framework the ground states of the even-N isotopes at $N > 126$ are determined by the filling of the lower lying $\nu i_{11/2}$ shell [5] in contradiction to the numerous shell-model calculations where the $\nu g_{9/2}$ orbital is fixed below the $\nu i_{11/2}$ one by 779 keV (see, for example, Refs. [65–67] and references therein). It should be noted, that these shell-model calculations quite successfully describe spectra and transition probabilities for the majority of the even-N nuclei in the vicinity of the shell closures at $N = 126$ and $Z = 82$. Evidently, the TFFS calculations with the Fayans functionals are free from these problems.

In Fig. 7 the experimental staggering indicator values for different isotopic chains are shown. The theoretical values are given only for the lead and thallium isotopes not to overburden the figure. Results for the other chains are similar to those for lead and thallium isotopes. As in the case of the kink, one can see the striking similarity in the staggering indicators

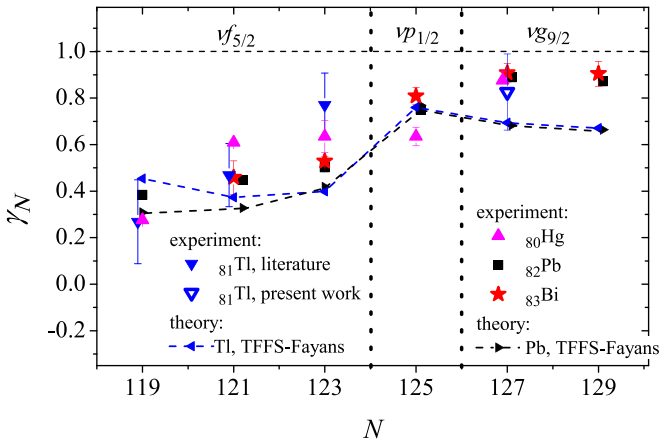

FIG. 7. Staggering indicator for the isotopic chains near $Z = 82$ and $N = 126$. Experimental data are taken from Refs. [7] (Pb isotopes); [3,5,6] (Hg isotopes); [8,58] (Bi isotopes); [56] and present work (Tl isotopes).

for $Z = 80, 81, 82, 83$. In particular, for each chain there is a clear dependence of γ_N on the shell occupied by the valence neutron ($\nu f_{5/2}$, $\nu p_{1/2}$, $\nu g_{9/2}$). The self-consistent TFFS calculations reproduce staggering indicator and its neutron-number dependence with the exception of the values at $N > 126$ when the $\nu g_{9/2}$ shell is filling. As it was shown in Ref. [41], the fluctuating contribution due to the quasiparticle-phonon interaction can be important for $N > N_{\text{magic}}$.

In the RMF calculations two different procedures labeled as "LES" and "EGS" were used for the blocking in odd-A nuclei [5,6]. In the LES procedure, the lowest-energy configuration was used, which is similar to the TFFS-Fayans calculations of OES [21,38]. In the EGS procedure, the configuration with the spin and parity of the blocked state corresponding to those of the experimental ground state is employed, although it is not necessarily the lowest in energy.

It was found that in the RMF approach the OES is described reasonably well when the EGS procedure is applied. With the LES procedure, the experimental OES is significantly underestimated [5,6]. At the same time, in the TFFS-Fayans calculations there are no additional conditions for the choice of the blocked state in the odd-N nuclei due to the good reproduction of the neutron single-particle spectrum in contrast with the RMF theory.

VI. CONCLUSION

The $\delta\langle r^2\rangle$ values for $^{207}\text{Tl}^m$ ($I^\pi = 11/2^-$) and $^{209}\text{Tl}^g$ ($I^\pi = 1/2^+$) have been measured for the first time, using laser resonance-ionization spectroscopy in the LIST ion source at ISOLDE (CERN). The characteristic kink in the ground-state thallium charge radii at the $N = 126$ shell closure has been observed. It was found that the kink indicator for thallium coincides within the limit of uncertainties with that for the neighboring mercury, lead, and bismuth isotopic chains. Thus, there is no notable difference between the cases where valence protons occupy low-j orbitals, such as in thallium ($s_{1/2}$), and high-j ones as in bismuth ($h_{9/2}$). The independence of the kink on the orbital occupied by the valence proton is supported by the negligible isomer shift for $^{207}\text{Tl}^m$ ($I = 11/2, \pi h_{11/2}$) relative to $^{207}\text{Tl}^g$ ($I = 1/2, \pi s_{1/2}$) (see Table I).

Measurement of the IS for ^{209}Tl also enabled us to complete the systematics in the OES in the considered region. As in the case of the kink, the OES for thallium isotopes near $N = 126$ coincides in the limits of uncertainties with that for the neighboring isotopic chains.

The detailed comparison of the complete set of the experimental $\delta\langle r^2\rangle$ data near $N = 126$, $Z = 82$ and the theory was made. Calculations using the DF3-a functional by Fayans *et al.* [21,36,37] with adjustment of parameters in the pairing sector demonstrate a good agreement with the experimental data for the S_n, kink and OES values in the mercury, thallium, lead, and bismuth chains with the exception of the OES at $N > 126$. The latter deficiency can be connected with neglecting the phonon coupling, which has an impact in this region [41].

The recent advanced RMF functionals (PC-L3R, PC-X, DD-MEX, and DD-PCX; see Ref. [33]) overestimate the kink-indicator value and show its Z dependence which is absent in experimental data. The very presence of the kink in the RMF theory is determined by the inversion of the position of the $\nu g_{9/2}$ and $\nu i_{11/2}$ neutron shells. In the TFFS-Fayans calculations the order of the single-particle neutron states near $N = 126$ corresponds well with the experimental data and there is no inversion of the $\nu g_{9/2}$ and $\nu i_{11/2}$ states. Further theoretical and experimental efforts are required in order to elucidate the influence of the neutron single-particle spectrum on the charge radius evolution. It should be noted that in contrast with our TFFS-Fayans calculations, the RMF functionals were not adjusted to provide the kink description in this specific mass region.

The complete set of data on charge radii in the close vicinity of magic $Z = 82$ and $N = 126$ helps to further elucidate the pairing part of the Fayans functional which would enable a better description of the kink and OES. Note, that other nuclear observables reveal more weak dependence on the gradient pairing strength [21]. The search for a universal parametrization in the pairing sector which would keep the global performance of the Fayans functional along with a good simultaneous description of the isotopic behavior for both geometric ($\delta\langle r^2\rangle$) and energetic (S_n) differential observables throughout the nuclide chart is the aim of future work.

ACKNOWLEDGMENTS

We would like to acknowledge the support of the ISOLDE collaboration and technical teams. The research leading to these results has received funding from the European Union's Horizon Europe Research and Innovation Programme under Grant Agreement No. 101057511. The work was supported by the STFC Grants No. ST/V001035/1, No. ST/V001108/1, No. ST/V001027/1, and No. ST/P004598/1, by the Romanian Nucleu Project No. PN 23 21 01 02 and IFA Grant No. CERN/ISOLDE, by the Research Foundation Flanders (FWO, Belgium), by BOF KU Leuven (Grant No. C14/22/104), by the Spanish funding agency MICIN/AEI 10.13039/501100011033 (FEDER, EU) via Projects No.

RTI2018-098868-B-I00 and No. PID2021-126998OB-I00, by German BMBF under Contract No. 05P21PKCI1 and Verbundprojekt 05P2021, and by the Polish National Science Center under Grant No. 2020/39/B/ST2/02346, by the Polish Ministry of Education and Science under Contract No. 2021/WK/07. M.A. acknowledges funding from the European's Union Horizon 2020 Research and Innovation Program under Grant Agreement No. 861198 project 'LISA' (Laser Ionization and Spectroscopy of Actinides) Marie Skłodowská-Curie Innovative Training Network (ITN).

[1] I. Angeli and K. Marinova, At. Data Nucl. Data Tables **99**, 69 (2013).
[2] X. Yang, S. Wang, S. Wilkins, and R. Garcia Ruiz, Prog. Part. Nucl. Phys. **129**, 104005 (2023).
[3] G. Ulm, S. K. Bhattacherjee, P. Dabkiewicz, G. Huber, H.-J. Kluge, T. Kühl, H. Lochmann, E.-W. Otten, K. Wendt, S. A. Ahmad, W. Klempt, R. Neugart, and ISOLDE Collaboration, Z. Phys. A **325**, 247 (1986).
[4] E. Verstraelen, A. Teigelhöfer, W. Ryssens, F. Ames, A. Barzakh, M. Bender, R. Ferrer, S. Goriely, P.-H. Heenen, M. Huyse, P. Kunz, J. Lassen, V. Manea, S. Raeder, and P. Van Duppen, Phys. Rev. C **100**, 044321 (2019).
[5] T. Day Goodacre, A. V. Afanasjev, A. E. Barzakh, B. A. Marsh, S. Sels, P. Ring, H. Nakada, A. N. Andreyev, P. Van Duppen, N. A. Althubiti, B. Andel, D. Atanasov, J. Billowes, K. Blaum, T. E. Cocolios, J. G. Cubiss, G. J. Farooq-Smith, D. V. Fedorov, V. N. Fedosseev, K. T. Flanagan *et al.*, Phys. Rev. Lett. **126**, 032502 (2021).
[6] T. Day Goodacre, A. V. Afanasjev, A. E. Barzakh, L. Nies, B. A. Marsh, S. Sels, U. C. Perera, P. Ring, F. Wienholtz, A. N. Andreyev, P. Van Duppen, N. A. Althubiti, B. Andel, D. Atanasov, R. S. Augusto, J. Billowes, K. Blaum, T. E. Cocolios, J. G. Cubiss, G. J. Farooq-Smith *et al.*, Phys. Rev. C **104**, 054322 (2021).
[7] M. Anselment, W. Faubel, S. Göring, A. Hanser, G. Meisel, H. Rebel, and G. Schatz, Nucl. Phys. A **451**, 471 (1986).
[8] A. E. Barzakh, D. V. Fedorov, V. S. Ivanov, P. L. Molkanov, F. V. Moroz, S. Y. Orlov, V. N. Panteleev, M. D. Seliverstov, and Y. M. Volkov, Phys. Rev. C **97**, 014322 (2018).
[9] V. S. Letokhov, V. I. Mishin, S. K. Sekatsky, V. N. Fedoseyev, G. D. Alkhazov, A. E. Barzakh, V. P. Denisov, and V. E. Starodubsky, J. Phys. G **18**, 1177 (1992).
[10] B. Pritychenko, M. Birch, B. Singh, and M. Horoi, At. Data Nucl. Data Tables **107**, 1 (2016).
[11] A. E. Barzakh, L. K. Batist, D. V. Fedorov, V. S. Ivanov, K. A. Mezilev, P. L. Molkanov, F. V. Moroz, S. Y. Orlov, V. N. Panteleev, and Y. M. Volkov, Phys. Rev. C **86**, 014311 (2012).
[12] A. E. Barzakh, L. K. Batist, D. V. Fedorov, V. S. Ivanov, K. A. Mezilev, P. L. Molkanov, F. V. Moroz, S. Y. Orlov, V. N. Panteleev, and Y. M. Volkov, Phys. Rev. C **88**, 024315 (2013).
[13] A. E. Barzakh, A. N. Andreyev, T. E. Cocolios, R. P. de Groote, D. V. Fedorov, V. N. Fedosseev, R. Ferrer, D. A. Fink, L. Ghys, M. Huyse, U. Köster, J. Lane, V. Liberati, K. M. Lynch, B. A. Marsh, P. L. Molkanov, T. J. Procter, E. Rapisarda, S. Rothe, K. Sandhu, M. D. Seliverstov, A. M. Sjödin, C. Van Beveren, P. Van Duppen, M. Venhart, and M. Veselský, Phys. Rev. C **95**, 014324 (2017).
[14] V. Fedosseev, K. Chrysalidis, T. D. Goodacre, B. Marsh, S. Rothe, C. Seiffert, and K. Wendt, J. Phys. G **44**, 084006 (2017).
[15] D. Fink, S. Richter, B. Bastin, K. Blaum, R. Catherall, T. Cocolios, D. Fedorov, V. Fedosseev, K. Flanagan, L. Ghys, A. Gottberg, N. Imai, T. Kron, N. Lecesne, K. Lynch, B. Marsh, T. Mendonca, D. Pauwels, E. Rapisarda, J. Ramos, R. Rossel, S. Rothe, M. Seliverstov, M. Sjödin, T. Stora, C. Van Beveren, and K. Wendt, Nucl. Instrum. Methods Phys. Res. B **317**, 417 (2013).
[16] D. A. Fink, T. E. Cocolios, A. N. Andreyev, S. Antalic, A. E. Barzakh, B. Bastin, D. V. Fedorov, V. N. Fedosseev, K. T. Flanagan, L. Ghys, A. Gottberg, M. Huyse, N. Imai, T. Kron, N. Lecesne, K. M. Lynch, B. A. Marsh, D. Pauwels, E. Rapisarda, S. D. Richter, R. E. Rossel, S. Rothe, M. D. Seliverstov, A. M. Sjödin, C. Van Beveren, P. Van Duppen, and K. D. A. Wendt, Phys. Rev. X **5**, 011018 (2015).
[17] R. Heinke, M. Au, C. Bernerd, K. Chrysalidis, T. E. Cocolios, V. N. Fedosseev, I. Hendriks, A. A. Jaradat, M. Kaja, T. Kieck, T. Kron, R. Mancheva, B. A. Marsh, S. Marzari, S. Raeder, S. Rothe, D. Studer, F. Weber, and K. Wendt, Nucl. Instrum. Methods Phys. Res. B **541**, 8 (2023).
[18] M. Sharma, G. Lalazissis, and P. Ring, Phys. Lett. B **317**, 9 (1993).
[19] N. Tajima, P. Bonche, H. Flocard, P.-H. Heenen, and M. Weiss, Nucl. Phys. A **551**, 434 (1993).
[20] P.-G. Reinhard and H. Flocard, Nucl. Phys. A **584**, 467 (1995).
[21] S. Fayans, S. Tolokonnikov, E. Trykov, and D. Zawischa, Nucl. Phys. A **676**, 49 (2000).
[22] J. Libert, B. Roussière, and J. Sauvage, Nucl. Phys. A **786**, 47 (2007).
[23] B. S. Reehal and R. A. Sorensen, Nucl. Phys. A **161**, 385 (1971).
[24] W. Horiuchi and T. Inakura, Phys. Rev. C **105**, 044303 (2022).
[25] P. M. Goddard, P. D. Stevenson, and A. Rios, Phys. Rev. Lett. **110**, 032503 (2013).
[26] H. Nakada and T. Inakura, Phys. Rev. C **91**, 021302(R) (2015).
[27] H. Nakada, Phys. Rev. C **100**, 044310 (2019).
[28] T. Naito, T. Oishi, H. Sagawa, and Z. Wang, Phys. Rev. C **107**, 054307 (2023).
[29] X. Roca-Maza, G. Colò, and H. Sagawa, Phys. Rev. C **86**, 031306(R) (2012).
[30] S. Goriely, Nucl. Phys. A **933**, 68 (2015).
[31] G. Lalazissis, S. Raman, and P. Ring, At. Data Nucl. Data Tables **71**, 1 (1999).
[32] U. C. Perera, A. V. Afanasjev, and P. Ring, Phys. Rev. C **104**, 064313 (2021).
[33] Z. X. Liu, Y. H. Lam, N. Lu, and P. Ring, At. Data Nucl. Data Tables **156**, 101635 (2024).
[34] A. Migdal, *Theory of Finite Fermi Systems and Applications to Atomic Nuclei* (Wiley, New York, 1967)
[35] S. Fayans and D. Zawischa, Phys. Lett. B **383**, 19 (1996).
[36] E. E. Saperstein and S. V. Tolokonnikov, Phys. At. Nucl. **74**, 1277 (2011).
[37] S. V. Tolokonnikov and E. E. Saperstein, Phys. At. Nucl. **73**, 1684 (2010).
[38] P.-G. Reinhard and W. Nazarewicz, Phys. Rev. C **95**, 064328 (2017).
[39] I. N. Borzov and S. V. Tolokonnikov, Phys. Part. Nucl. **54**, 586 (2023).

[40] A. Koszorús, X. F. Yang, W. G. Jiang, S. J. Novario, S. W. Bai, J. Billowes, C. L. Binnersley, M. L. Bissell, T. E. Cocolios, B. S. Cooper, R. P. de Groote, A. Ekström, K. T. Flanagan, C. Forssén, S. Franchoo, R. F. G. Ruiz, F. P. Gustafsson, G. Hagen, G. R. Jansen, A. Kanellakopoulos, M. Kortelainen, W. Nazarewicz, G. Neyens, T. Papenbrock, P.-G. Reinhard, C. M. Ricketts, B. K. Sahoo, A. R. Vernon, and S. G. Wilkins, Nat. Phys. **17**, 439 (2021).

[41] E. E. Saperstein, I. N. Borzov, and S. V. Tolokonnikov, JETP Lett. **104**, 218 (2016).

[42] I. N. Borzov and S. V. Tolokonnikov, Phys. At. Nucl. **83**, 828 (2020).

[43] R. P. de Groote, J. Billowes, C. L. Binnersley, M. L. Bissell, T. E. Cocolios, T. Day Goodacre, G. J. Farooq-Smith, D. V. Fedorov, K. T. Flanagan, S. Franchoo, R. F. Garcia Ruiz, W. Gins, J. D. Holt, A. Koszorús, K. M. Lynch, T. Miyagi, W. Nazarewicz, G. Neyens, P.-G. Reinhard, S. Rothe, H. H. Stroke, A. R. Vernon, K. D. A. Wendt, S. G. Wilkins, Z. Y. Xu, and X. F. Yang, Nat. Phys. **16**, 620 (2020).

[44] C. Gorges, L. V. Rodríguez, D. L. Balabanski, M. L. Bissell, K. Blaum, B. Cheal, R. F. Garcia Ruiz, G. Georgiev, W. Gins, H. Heylen, A. Kanellakopoulos, S. Kaufmann, M. Kowalska, V. Lagaki, S. Lechner, B. Maaß, S. Malbrunot-Ettenauer, W. Nazarewicz, R. Neugart, G. Neyens, W. Nörtershäuser, P.-G. Reinhard, S. Sailer, R. Sánchez, S. Schmidt, L. Wehner, C. Wraith, L. Xie, Z. Y. Xu, X. F. Yang, and D. T. Yordanov, Phys. Rev. Lett. **122**, 192502 (2019).

[45] M. Kortelainen, Z. Sun, G. Hagen, W. Nazarewicz, T. Papenbrock, and P.-G. Reinhard, Phys. Rev. C **105**, L021303 (2022).

[46] W. Nörtershäuser and I. D. Moore, in *Handbook of Nuclear Physics*, edited by I. Tanihata, H. Toki, and T. Kajino (Springer Nature, Singapore, 2022), pp. 1–70.

[47] S. E. Agbemava, A. V. Afanasjev, D. Ray, and P. Ring, Phys. Rev. C **89**, 054320 (2014).

[48] Z. X. Liu, Y. H. Lam, N. Lu, and P. Ring, Phys. Lett. B **842**, 137946 (2023).

[49] A. Taninah, S. Agbemava, A. Afanasjev, and P. Ring, Phys. Lett. B **800**, 135065 (2020).

[50] E. Yüksel, T. Marketin, and N. Paar, Phys. Rev. C **99**, 034318 (2019).

[51] Z. Yue, A. Andreyev, A. Barzakh, I. Borzov, J. Cubiss, A. Algora, M. Au, M. Balogh, S. Bara, R. Bark, C. Bernerd, M. Borge, D. Brugnara, K. Chrysalidis, T. Cocolios, H. De Witte, Z. Favier, L. Fraile, H. Fynbo, A. Gottardo *et al.*, Phys. Lett. B **849**, 138452 (2024).

[52] ISOLDE Decay Station, https://isolde-ids.web.cern.ch/, accessed online April 5, 2024.

[53] G. Hermann, G. Lasnitschka, and D. Spengler, Z. Phys. D **28**, 127 (1993).

[54] National Nuclear Data Center, https://www.nndc.bnl.gov/ensdf/, accessed online April 5, 2024.

[55] W. Lauth, H. Backe, M. Dahlinger, I. Klaft, P. Schwamb, G. Schwickert, N. Trautmann, and U. Othmer, Phys. Rev. Lett. **68**, 1675 (1992).

[56] G. Penyazkov, S. D. Prosnyak, A. E. Barzakh, and L. V. Skripnikov, J. Chem. Phys. **158**, 114110 (2023).

[57] E. W. Otten, in *Treatise on Heavy Ion Science: Volume 8: Nuclear Far From Stability*, edited by D. A. Bromley (Springer, Boston, MA, 1989), pp. 517–638.

[58] M. R. Pearson, P. Campbell, K. Leerungnavarat, J. Billowes, I. S. Grant, M. Keim, J. Kilgallon, I. D. Moore, R. Neugart, M. Neuroth, S. Wilbert, and the ISOLDE Collaboration, J. Phys. G **26**, 1829 (2000).

[59] I. N. Borzov, S. A. Fayans, E. Krömer, and D. Zawischa, Z. Phys. A **355**, 117 (1996).

[60] V. A. Khodel, A. P. Platonov, and E. E. Saperstein, J. Phys. G **8**, 967 (1982).

[61] M. Wang, W. Huang, F. Kondev, G. Audi, and S. Naimi, Chin. Phys. C **45**, 030003 (2021).

[62] Y. Tanimura and M.-K. Cheoun, Phys. Rev. C **109**, 054323 (2024).

[63] E. V. Litvinova and A. V. Afanasjev, Phys. Rev. C **84**, 014305 (2011).

[64] A. V. Afanasjev and E. Litvinova, Phys. Rev. C **92**, 044317 (2015).

[65] B. Andel, P. Van Duppen, A. N. Andreyev, A. Blazhev, H. Grawe, R. Lică, H. Naïdja, M. Stryjczyk, A. Algora, S. Antalic, A. Barzakh, J. Benito, G. Benzoni, T. Berry, M. J. G. Borge, K. Chrysalidis, C. Clisu, C. Costache, J. G. Cubiss, H. De Witte *et al.*, Phys. Rev. C **104**, 054301 (2021).

[66] B. Andel, A. N. Andreyev, A. Blazhev, R. Lică, H. Naïdja, M. Stryjczyk, P. Van Duppen, A. Algora, S. Antalic, A. Barzakh, J. Benito, G. Benzoni, T. Berry, M. J. G. Borge, K. Chrysalidis, C. Clisu, C. Costache, J. G. Cubiss, H. De Witte, D. V. Fedorov *et al.*, Phys. Rev. C **109**, 064321 (2024).

[67] S. Shukla, P. C. Srivastava, and D. Patel, J. Phys. G **51**, 075103 (2024).